2013, Scienceline Publication

Journal of Civil Engineering and Urbanism

JCEU

Volume 3, Issue 4: 142-149 (2013) (Received: November 18, 2012; Accepted: April 23, 2013; Published: July 30, 2013) ISSN-2252-0430

Study of Slope Stability and Failure Process of Rock-Fill Barriers

Farzaneh Ghaderi Nasab [1], Ebrahim Amiri Tokaldany[*2] and Mohammad Hadi Davoudi [3]

[1]*Department of Irrigation and Reclamation Engineering, Faculty of Agricultural Engineering and Technology, University of Tehran, Karaj, Iran*
[2]*Associate Professor, Department of Irrigation and Reclamation Engineering, Faculty of Agricultural Engineering and Technology, University of Tehran, Karaj, Iran.*
[3]*Associate Professor, Soil Conservation and Watershed Management Research Institute, Tehran, Iran,*

*Corresponding Author's E-mail address: amiri@ut.ac.ir

ABSTRACT: A rock-fill barrier is an economical and effective structure for flood routing as well as stabilizing river bed and banks. Rock-fill barrier is a permeable and flexible structure and could resist against forces due to flow through and over flow from this structure. This study was carried out to investigate the failure process and providing criteria for slope stability of rock-fill barriers. Eighty-eight laboratory tests were performed in a flume with a longitudinal slope of 0.003 m/m, width of 0.6m, height of 0.8m and length of 14 m. A dimensional analysis technique was used to develop equations for calculating values of depth of flow in the upstream side of the barrier, the maximum flow under which a barrier remains stable, and evaluation for downstream stability of side slopes in terms of discharge, gradation of material, standard deviation of material size and upstream and downstream water depths. Data from laboratory tests were used to evaluate the results of the new equations. Using the criteria of mean relative error and root-mean-square error, it is found that there is a good accuracy of the equations introduced in this research.

Keywords: Stability, Failure, Pervious Barrier, Flood Control, Through-Flow And Over Flow Capacity

ORIGINAL ARTICLE

INTRODUCTION

Rock-fill barriers are used for flood control in watershed management. They are economical and effective structures for flood detention and control purposes in situations when rock is readily available (Heydari and Hosseinzadeh Talaee, 2011). The objectives of constructing rock-fill detention barriers are flow storage for a specific period and lowering an outflow hydrograph (Samani and Heydari, 2007). The ancillary advantages of this kind of structure are flexibility, durability, permeability and economy (Leu et al., 2008). This type of structure is considered environmentally friendly because its permeability allows small particles and aquatic life to pass through longitudinally (Michioku et al., 2005). Rock-fill barriers filter some sediment from runoff, which serves to reduce erosion and sediment transportation downstream from the structure.

In terms of hydraulic behavior, rock-fill barriers are very complicated structures as the flow that passes through and over them is inherently turbulent and non-Darcy (Li et al., 1998; Hansen and Bari, 2002; Zeng and Grigg, 2006 and Sidiropoulou et al., 2007), and sediment is able to pass through in a downstream direction (Mousavi et al., 2011 and Nazemi et al., 2011). Furthermore, overflow may occur simultaneously with through flow. Tests performed by Macintosh (2004), showed that there was a significant interaction between seepage and overflow, particularly for small to medium floods, and concluded that interactions between seepage and overflow cannot be ignored (Chanson, 2009). Also, there is the possibility that due to collision among stones and the interaction between stones and fluid, stones may move and the barrier is destroyed. For these reasons, less theoretical and experimental attentions have been paid to the stability of these barriers.

Mohamed (2010) performed a series of laboratory experiments in order to investigate flow through and over gabion weirs and developed empirical Equations (1) and (2) for computing the amounts of discharge from gabion weirs at both free surface and submerged flow conditions, respectively:

$$\frac{Q_f}{\sqrt{g}By_1^{1.5}} = -0.37 + 0.095\log Re + 0.063\frac{H}{L} + 0.114\frac{d}{P} \qquad (1)$$

$$\frac{Q_s}{\sqrt{g}By_1^{1.5}} = -0.41 + 0.105\log Re + 0.031\frac{H}{L} + 0.057\frac{d}{P} + 0.018s_r \qquad (2)$$

where $S_r=(y_1-y_2)/H$ which y_1 and y_2 are upstream and downstream water depths (m), respectively and H is the water head above the weir (m); $Re= Q\square /B\square$ in which $\square$ is the fluid density (kg m^{-3}) and $\square$ is the dynamic viscosity of the fluid (kg $m^{-1}s^{-1}$); Q_f is discharge at free surface condition (m^3 s^{-1}); Q_s is discharge at submerged flow condition (m^3 s^{-1}); B is the channel width (m); P is the weir height (m); L is the width of the weir in the direction of flow (m); g is gravity of acceleration (m s^{-2}); d is the mean stone size used in gabion construction (m).

Lenzi (2002) in a study for stability analysis of low-check dams, constructed by boulders and used for river bed slope control as well as river bed stabilization, proposed the following equation to assess the near bed sliding velocity of stone particles (V_f).

$$V_f = \sqrt{\frac{2(\rho_s-\rho)g\beta(f\cos\alpha-\sin\alpha)D_x}{C_D\rho}} \qquad (3)$$

Where C_D is the coefficient of hydrodynamic resistance (-); $\square_s$ is the stone density (kg m^{-3}); D_x is the

length of stone in the direction of flow (m); □ is the shape parameter (-); □ is the angle of placement of stone (degrees); and *f* is the friction coefficient (-).

Maeno et al. (2002) conducted experiments to investigate the basic hydraulic characteristics of a rubble mound weir. According to the results of Maeno et al. 2002's experiments, the tractive force as well as the seepage force, are factors that may contribute to early stage failure of the downstream slope of a rubble mound weir.

Although some design aspects of rock-fill barriers for both over and through flows have been investigated by those aforementioned researchers, there are more aspects have to be addressed for a safe design of these structures; such as determination of through and overflow capacities, prediction of upstream flow depth, stability of barriers in terms of downstream side slopes, and also their response during a distractive flood. In this research, we aimed to introduce some criteria regarding a safe design of rock-fill dams in terms of upstream water depth, gradation of the stones, and the geometry of the dams. In this regard we conducted a set of laboratory experiments using a model of rock-fill dam constructed in a laboratory flume. In next chapter, the experimental setup and the methods to collect data have been introduced.

MATERIAL AND METHODS

Laboratory experiments were carried out in a flume at the Soil Conservation and Watershed Management Research Institute, Tehran, Iran. Dimensions of the flume in terms of length, height and width were 14m×0.8m×0.6m, respectively. The flume was capable of being operated with discharge amounts of up to 85 lit/s from a water circulation system, which was fed by two pumps.

Eighty-eight physical models of rock-fill barrier were made of eight grades of material with various downstream side slopes from 1V:2.5H to 1V:6H (where V and H represent vertical and horizontal directions, respectively). All models were 50 cm in height; had 100 cm crest width and 1V:2H upstream side slope. In order to investigate the particle-size distribution of stone mixtures, particle mean diameter and standard deviations of particle size, were calculated according to Herrera and Felton (1991), and are shown in Eqs. (4) and (5):

$$d = \frac{\sum d_i w_i}{\sum w_i} \quad (4)$$

$$\sigma = \left[\frac{\sum (d-d_i)^2 w_i}{\sum w_i}\right]^{0.5} \quad (5)$$

Where d is the mean diameter of stone (m), d_i is the mean diameter of two sequential sieves (m); w_i is the percentage of stone between two sequential sieves, and □□is the standard deviation of stone. Table 1 shows percentages of graded stone for reaching desired gradation levels in mixtures.

To measure water depth in the body of the dam, a series of piezometers was installed on the flume bed along the model and in the direction of the flow. A rectangular weir was used at the downstream end of the flume to measure the rate of discharge flow. Two point gages were used upstream and downstream of the barrier to record the water levels. Using the upstream point gage, water level (y_1) at positions of one to four times of the maximum water depth over the barrier were measured and recorded at the upstream of the barrier. Figure 1 presents a schematic plan of the setup used in this research.

Table 1. Percentage of graded stones in the mixture

Sieve size (cm)	0.7	1.7	2.8	3.7	4.44	5.8	6.4	7.62	8.9	9.8	11	12	13	Gradation	
														d(cm)	s(cm)
w_i (%)				11	20	15	12	13	19	10				7	2
w_i (%)					8	20	48	16	8					7	1
w_i (%)						10.5	79	10.5						7	0.5
w_i (%)	20	14	11	15	10	15	15							4	2
w_i (%)		12	28	30	21	9								4	1
w_i (%)			20	64	16									4	0.5
w_i (%)							20	10	12	18	16	24		10	2
w_i (%)								15	30	30	25			10	1

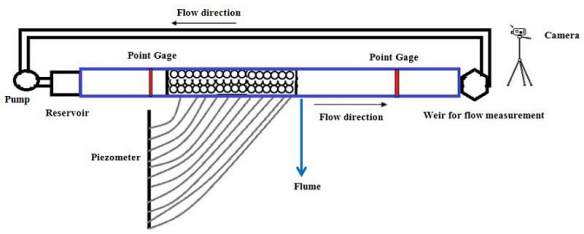

Figure1. Schematic plan of hydraulic laboratory instruments

For preparation of each physical model of the rock-fill barrier, rock particles were dumped randomly in the flume, and then formed according to the desired geometry. Before starting each experiment, an exact profile of the barrier was measured using a "Profile Indicator" in 3 axes along the direction of the flow (Figure 2).

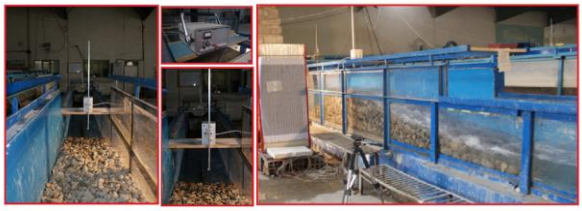

Figure2. Profile indicator to recording the geometry of the barrier

RESUTS AND ANALYSIS

Prediction for flow depth at the upstream of the barrier

As one of the aims in this research we investigated for the flow depth at the upstream of the barrier. Considering analytical investigation and experimental data presented in the cited literature, the functional relationship of upstream water depth y_1 may be expressed by:

$$y_1 = f_1(y_2, \alpha, \alpha_0, w_{top}, P, s, \sigma, d, B, a, b, c, Q, g, \mu, \rho_s, \rho, n_{man}) \quad (6)$$

Where y_1 and y_2 are water depths upstream and downstream of the barrier (L), respectively; □□ and □$_0$ are upstream and downstream side slope angles of the barrier (degrees), respectively; w_{top} is the crest width of the barrier (in the direction of channel flow, L); P is the height of the barrier (L); s is the longitudinal slope of the open channel (L/L); □ is the standard deviation of stone (L), d is the mean diameter of stone (L), B is the width of channel (L); a, b and c represent sizes of stone in three of axes (L); Q is the discharge (L^3 T^{-1}); and n_{man} is Manning's roughness coefficient. In Figure 3 some of the effective parameters are shown:

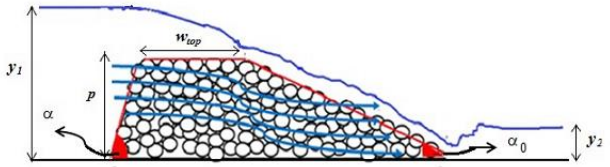

Figure3. Definition sketch to show some of the effective parameters: y_1 and y_2 are water depths upstream and downstream of the barrier (L), respectively; □□ and □$_0$ are upstream and downstream side slope angles of the barrier (degrees), respectively; w_{top} is the crest width of the barrier (in the direction of channel flow, L); P is the height of the barrier (L);

Using Buckingham's □ theorem (Streeter and Wylie, 1998) of dimensional analysis and also some transformations, leads to the non-dimensional relation as:

$$\frac{y_1}{P} = f_1(\tan\alpha, \tan\alpha_0, n_{man}, s, \frac{w_{top}}{P}, \frac{d-\sigma}{d}, \frac{d}{P}, Re, fr, \frac{B}{P}, \frac{\rho_s}{\rho}, \frac{c}{\sqrt{ab}}) \quad (7)$$

Where $fr = q/(g{y_2}^{3)(1/2)}$ and $Re = q$□/□. After passing up the constant parameters; i.e tan□, n_{man}, s, w_{top}/P, B/P, □$_s$/□, $c/(ab)^{0.5}$, a multiple nonlinear regression analysis is used to correlate all dimensionless parameters shown in Eq. (7) to develop an empirical equation for prediction of depth of flow in barrier upstream as follows:

$$\frac{y_1}{P} = a(\tan\alpha_0)^b Re^c fr^d \left(\frac{d-\sigma}{d}\right)^e \left(\frac{d}{P}\right)^f \quad (8)$$

To find out the constant parameters in Eq. (8); a, b, c, d, e, and f, we carried out a set of experiments in which the amount of discharge was gradually increased in several steps and records were taken for water levels upstream and downstream of the barrier once they have reached to a fix level. The amounts of the considered parameters were estimated from the statistical analysis of data obtained from 250 tests over different models, and employing SPSS software. The final equation to determine the depth of flow in upstream of barrier can be written as:

$$\frac{y_1}{P} = 0.003(\tan\alpha_0)^{-0.055} Re^{0.411} fr^{-0.778} \left(\frac{d-\sigma}{d}\right)^{-0.128} \left(\frac{d}{P}\right)^{-0.166} \quad (9)$$

To evaluate Eq. (9) for predictions of upstream water levels, 130 tests were done. Result of experiments and the corresponding results from Eq. (9) were compared together and a fair correlation was observed between two sets of data (Figure 4).

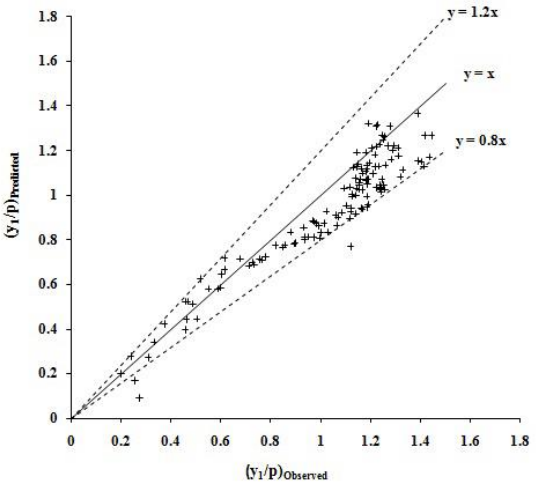

Figure4. Validation of Eq. (9) to predict the depth of flow at the upstream of the barrier: $(y_1/p)_{Observed}$ is the value observed in experiment and $(y_1/p)_{Predicted}$ is the value predicted by Eq. (9), where y_1 is water depths upstream of the barrier and P is the height of the barrier.

The accuracy of Eq. (9) was determined by computing the mean relative error (*MRE*) and the root-mean –square error (*RMSE*) using following equations:

$$MRE = \frac{1}{n}\sum \frac{Observed_{(i)} - Predicted_{(i)}}{Observed_{(i)}} \quad (10)$$

$$RMSE = \left[\frac{\sum_{i=1}^{N}(Observed_{(i)} - Predicted_{(i)})^2}{n}\right]^{0.5} \quad (11)$$

Where n is the number of tests, and $Observed_{(i)}$ and $Predicted_{(i)}$ are observed and predicted values of parameters of interest, respectively.

Using Eqs. (10) and (11), *MRE* and *RMSE* were determined as 0.075 and 0.074, respectively, indicating a good agreement with the results of Eq. (9) and values observed from the experiments.

The effect of standard deviation of stone on water level at barrier upstream

Figure 5 shows the variation of upstream water depth via discharge per unit width for two types of models with the same geometry and mean diameter of stone, but at different standard divisions of stone; i.e. 0.5 and 2cm. Figure 5 shows that increasing the standard deviation of stones results in an increase in upstream water depth for the same discharge. Moreover, considering the barrier height, Figure 5 indicates that in cases of no overflow, the variation of upstream depth is very sensitive to the variation of discharge until water levels reach to the crest level of the barrier.

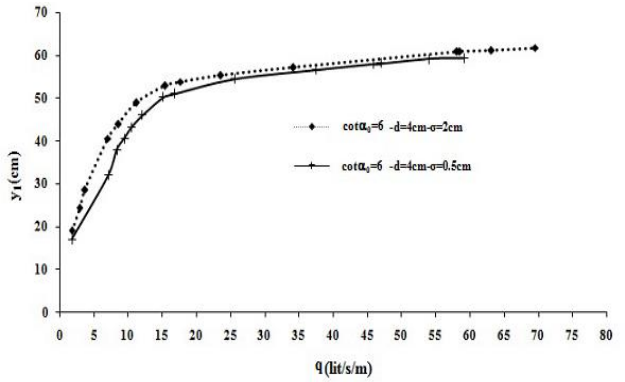

Figure5. The variation of upstream water depth versus discharge per unit width for different standard deviation of stone: y_1 is water depths upstream of the barrier(cm); q is the discharge per unit width (lit/s/m); cotα_0 is the cotangent(α_0); d is the mean diameter of stone (cm); σ is the standard deviation of stone (cm).

The effect of downstream side slope on upstream water level

Figure 6 shows the variations of upstream water depth against discharge per unit width for two types of model with the same gradation of stone, but different geometry. From Figure 6 it can be seen that the water depth upstream increases by decreasing the downstream side slope; i.e. increasing the size of barrier dimensions.

The effect of size of stone on water level in upstream

In Figure 7 the variations of upstream water depth against discharge per unit width for three models with the same geometry but different sizes of stones is shown. According to Figure 7 it can be seen that the upstream water depth increases by decreasing the size of stones.

Maximum flow under which the barrier remains stable (Q_0)

In the second series of the experiments, we focused on the study of the stability of rock-fill barriers. The process of programming these experiments is illustrated in Figure 8. Note that in each test and for each discharge, records were taken for upstream and downstream water levels as well as the elevation of water head in piezometers. Figure 9 shows one of the tests with a mean diameter of 10 cm, standard diviation of 2 cm, height of 48 cm, crest width of 100 cm, upstream side slope 1v:2H and downstream side slope 1V:3H. The discharge, Q_0, in which the barrier remained stable, was determined as 45 lit/s (Figure 9).

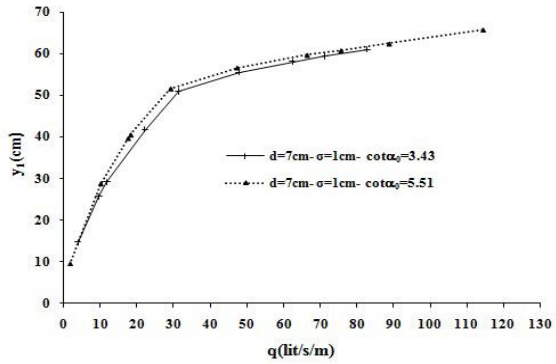

Figure6. The variation of upstream water depth versus discharge per unit width for downstream side slope angle.

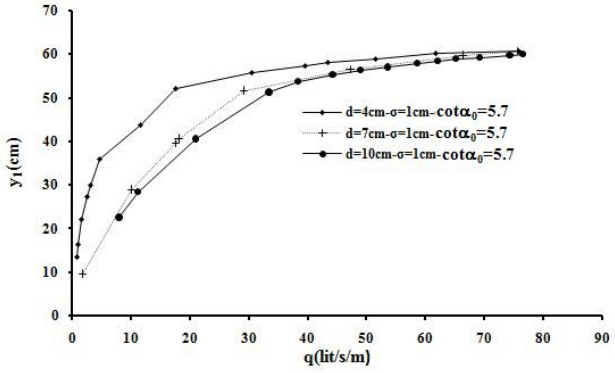

Figure7. The variation of upstream water depth versus discharge per unit width for mean diameter of sone.

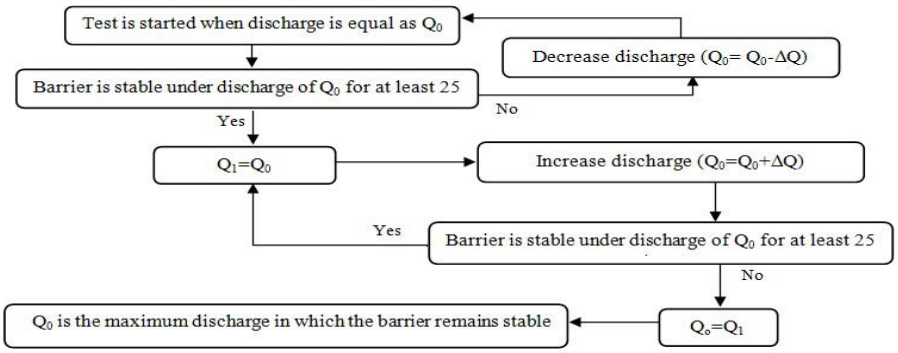

Figure 8. Schematic illustration of the experiment programming to find the maximum flow rate under which the barrier is still remained stable.

To cite this paper: F.Ghaderi Nasab, E. Amiri Tokaldany, M. H. Davoudi. 2013. Study of slope stability and failure process of rock-fill barriers. *J. Civil Eng. Urban*, 3(4): 142-149. http://www.ojceu.ir/main/

Figure9. An example to determine Q_0 for a series of data

In Figure 10, the maximum discharge per unit width under which the barrier remains stable (Q_0) for a specific geometry but different values for particle size and standard deviation are shown. Figure 10 demonstrates that Q_0 increases with an increase in the size of stone or a decrease in the downstream side slope. Moreover, Q_0 decreases with an increase of the standard deviation of the stones.

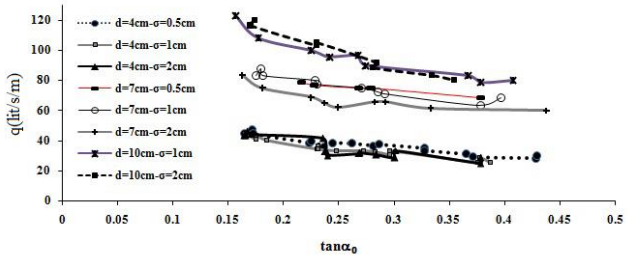

Figure10. summary of result of the experiment on maximum discharge per unit width under which the barrier is still remained stable (Q_0

Developing an equation for stable downstream side slope

Since flow is highly turbulent across rock-fill barriers, the influence of viscous forces is negligible in comparison to inertia forces. Moreover, as dynamic viscosity (□□ appears only in Reynolds number, *Re*, this number must not be present in turbulent filtration through the barrier (Yalin, 1971). The functional relationship for downstream stable side slope, $\square_0$, may be expressed by:

$$\alpha_0 = f_1\left(y_2, \alpha, w_{top}, P, s, \sigma, d, B, a, b, c, Q, g, \rho_s, \rho, n_{man}\right) \quad (12)$$

Using the Buckingham π theorem of dimensional analysis and some transformations, an empirical equation was developed for computing the stable downstream side slope as follows:

$$\tan\alpha_0 = b_1(\tan\alpha)^{b_2}\left(\frac{q}{\sqrt{g\frac{\rho_s-\rho}{\rho}d^3}}\right)^{b_3}\left(\frac{d}{P}\right)^{b_4}\left(\frac{\sigma}{d}\right)^{b_5}\left(\frac{w_{top}}{B}\right)^{b_6}\left(\frac{P}{B}\right)^{b_7}\times \left(\frac{y_1-y_2}{P}\right)^{b_8}(n_{man})^{b_9}s^{b_{10}}\left(\frac{c}{\sqrt{ab}}\right)^{b_{11}} \quad (13)$$

By considering all constant parameters as a single constant parameter, the following equation for computing the stable downstream side slope is introduced:

$$\tan\alpha_0 = a\left(\frac{d}{P}\right)^{b}\left(\frac{d-\sigma}{d}\right)^{c}\left(\frac{y_1-y_2}{P}\right)^{d}\left(Fr_{s,er}\right)^{e} \quad (14)$$

Where $Fr_{s,er}$ is considered as erosion-critical stone-referred Froude number equal to $q/(g(\square_s\text{-}\square_w)/\square_w d^3))^{0.5}$.

Values *a*, *b*, *c*, *d*, and *e* were estimated using statistical analysis by employing SPSS software for data obtained from 60 laboratory tests. The final equation to determine the stable downstream side slope of the barrier is as follows:

$$\tan\alpha_0 = 0.028\left(\frac{d}{P}\right)^{-0.847}\left(\frac{d-\sigma}{d}\right)^{0.307}\left(\frac{y_1-y_2}{P}\right)^{-2.328}\left(\frac{q}{\sqrt{g\frac{\rho_s-\rho}{\rho}d^3}}\right)^{-1.468} \quad (15)$$

In order to evaluate Eq. (15), the results obtained from other 28 laboratory tests were used and compared with those that resulted from Eq. (15). We found a reasonable agreement between these two groups of data (Figure 11).

Equations (10) and (11) were used to determine the amounts of *MRE* and *RMSE* as 0.09 and 0.04, respectively, indicating a good agreement between results obtained from Eq. (15) and those observed from laboratory experiments.

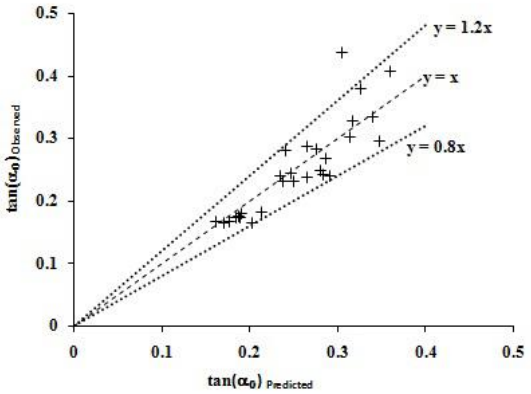

Figure11. Predicted values of downstream side slopes using Eq. (15) versus observed data: tan($\square_0$) Observed is the value observed in experiment and tan($\square_0$) Predicted is the value predicted by Eq. (15), where tan($\square_0$) is tangent($\square_0$) and $\square_0$ is downstream side slope angle

Mechanism of destruction of the barriers due to extra flow ($Q > Q_0$)

Effective design of porous barriers requires an understanding of the mechanism of destruction caused by flooding in these structures. For this purpose, tests were done on the deformation of the barrier body during a flow larger than Q_0. In these tests, for each flow and after a period of at least 25 minutes, flow was stopped and the geometry of the barrier was recorded with a profile indicator (Figure 12). For one of the tests, for instance, the failure of the model begins with moving stones along the downstream slope and changing the downstream slope to a milder one. The destruction of barriers continued until the collapsing stage and was followed by a stable stage.

Figure12. Failure process of the barrier foundation due to increasing flow

To cite this paper: F.Ghaderi Nasab, E. Amiri Tokaldany, M. H. Davoudi. 2013. Study of slope stability and failure process of rock-fill barriers. *J. Civil Eng. Urban*, 3(4): 142-149. http://www.ojceu.ir/main/

Figure 13 shows the deformation of a model at four destructive flow levels, with mean diameter and standard deviation of stones of 4cm and 0.5cm, respectively, height of 48cm, crest width of 100 cm, upstream side slope of 1V:2H, and downstream side slope of 1V:3.81H.

The model remained stable at a flow rate of 23lit/s, as shown in Figure 13. By increasing the rate of flow, a small amount of erosion took place and the crest width decreased. Finally, the downstream side slope of the model changed to form a milder slope as shown in Figure 13.

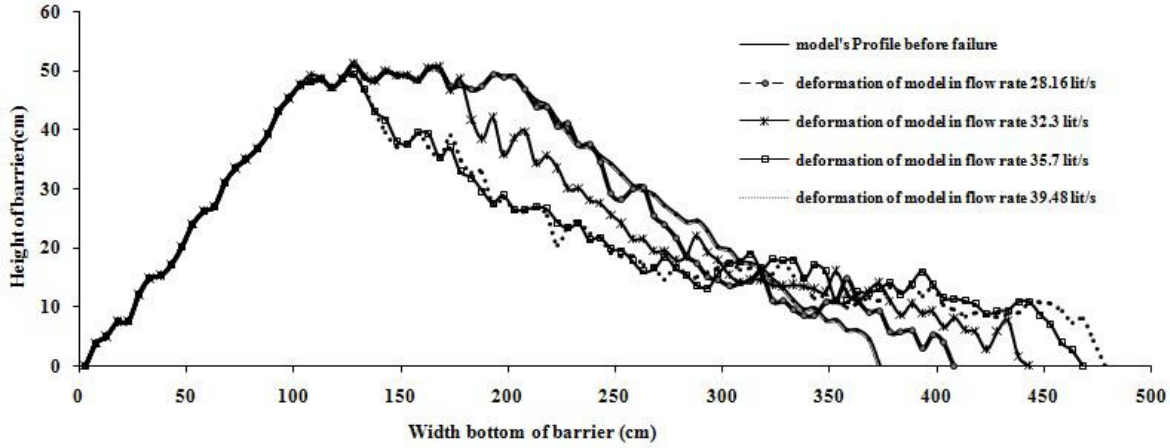

Figure 13. An example of the process of a barrier deformation

To obtain an equation to find the equilibrium downstream side slope of porous barriers in distractive flow ($\cot\alpha_n$), the functional relationship may be expressed by:

$$\cot\alpha_n = f_1(\cot\alpha_0, Q_0, Q_n, w_0, w_n, \sigma, d, \rho, \rho_s) \qquad (16)$$

Where α_n is the downstream side slope angle after deformation of the barrier; Q_n is the destructive flow that deforms the barriers, and w_n is the width crest of barriers after deformation.

Using Buckingham's π theorem of dimensional analysis together with some transformation, the following non-dimensional relation has been developed:

$$f_1\left(\frac{\cot\alpha_n}{\cot\alpha_0}, \frac{Q_n}{Q_0}, \frac{w_n}{w_0}, \frac{\rho}{\rho_s}, \frac{d-\sigma}{d}\right) = 0 \qquad (17)$$

A multiple nonlinear regression analysis was used to correlate all dimensionless parameters shown in Eq. (17) as follows:

$$\frac{\cot\alpha_n}{\cot\alpha_0} = a\left(\frac{Q_n}{Q_0}\right)^b\left(\frac{d-\sigma}{d}\right)^c\left(\frac{w_n}{w_0}\right)^d \qquad (18)$$

To find the constant values of *a*, *b*, *c*, and *d* in Eq. (18), a set of experiments was done and measurements were taken for downstream stable side slope after the destraction process (Figure 14). Due to water supply restrictions, more tests were made with smaller stones having a mean dimeter of 4 cm (Figure 15).

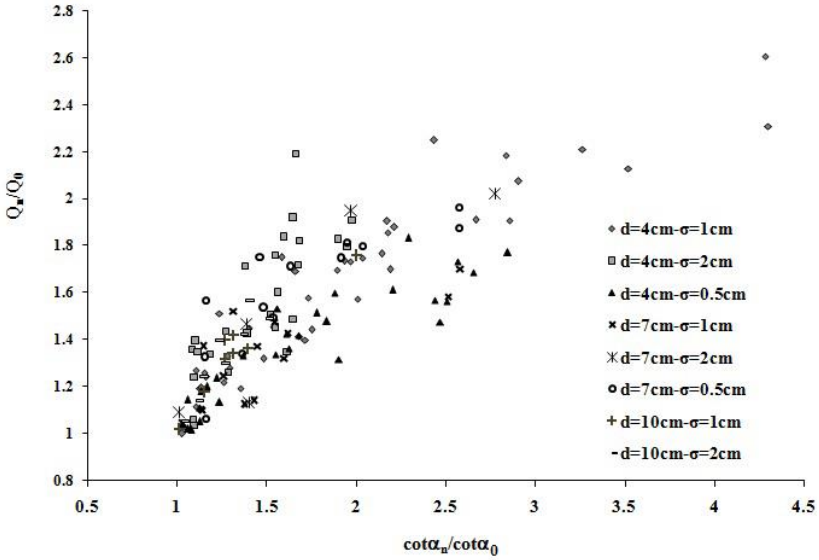

Figure14. Summary of the result of the experiment on the destruction mechanism of a barrier due to flooding ($Q > Q_0$): Q_0 is maximum discharge under which the barrier is still remained stable; α_0 is downstream side slope angle; α_n is the downstream side slope angle after deformation of the barrier; Q_n is the destructive flow that deforms the barriers.

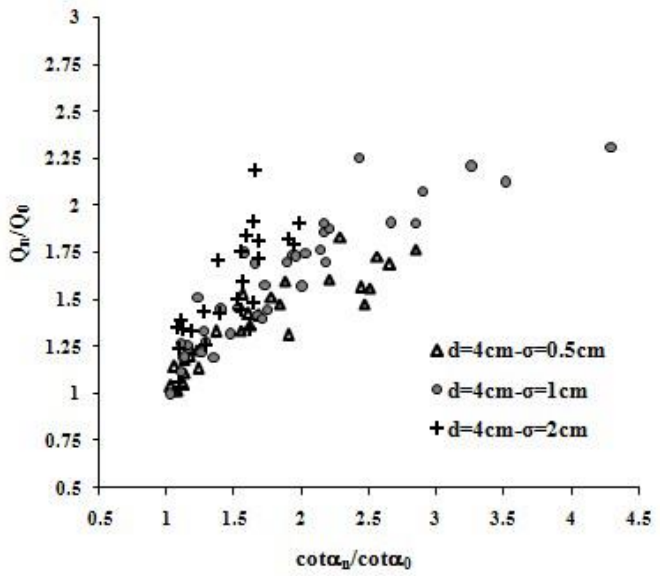

Figure15. Summary of the result of the experiments on the destruction mechanism of the barrier due to flooding ($Q > Q_0$) on stones having a mean diameter of 4cm:

Figure 15 shows that barriers composed of stones with bigger standard deviations experienced less deformation than those made of stones with lower standard deviation. Figure 16 demonstrates two models with the same geometry and size but with different levels of standard deviation after four flood events larger than Q_0. Figure 16 indicates that despite larger flow, the deformation of the model composed of stones with larger standard deviation was less than that of the model with lower standard deviation.

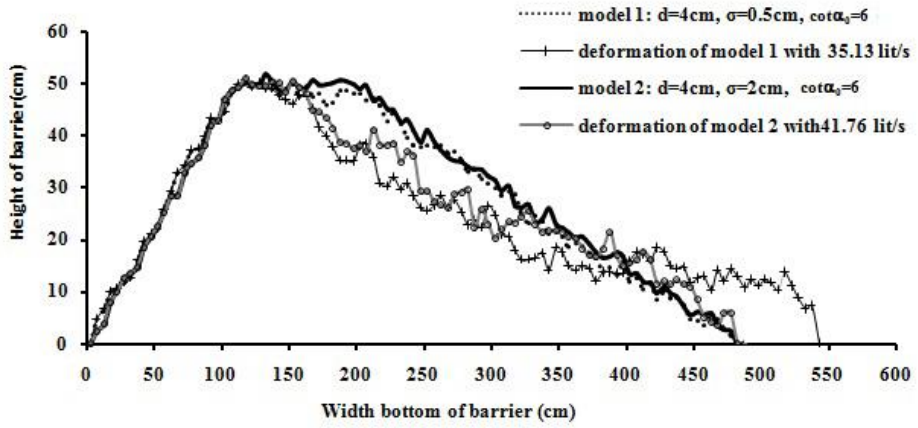

Figure 16. Deformation of 2 models with the same geometry and mean stone diameter but different standard deviations

A large number of experiments (neary 100) were done to estimate values of *a*, *b*, *c* and *d* using statistical analysis and employing SPSS software. Hence, the final equation to determine the stable downsteam side slope after deformation can be written as:

$$\frac{\cot\alpha_n}{\cot\alpha_0} = 1.163\left(\frac{Q_n}{Q_0}\right)^{0.915}\left(\frac{d-\sigma}{d}\right)^{0.321}\left(\frac{w_n}{w_0}\right)^{-0.194} \quad (19)$$

To evaluate Eq. (19), data obtained from 30 more experiments were compared with the corresponding results of the equation and a fair correlation was observed (Figure 17). The accuracy of Eq. (19) was determined using Eqs. (10) and (11); *MRE* and *RMSE* were determined as 0.14 and 0.307, respectively, indicating a good agreement with the results of Eq. (19)) and values observed in the experiments.

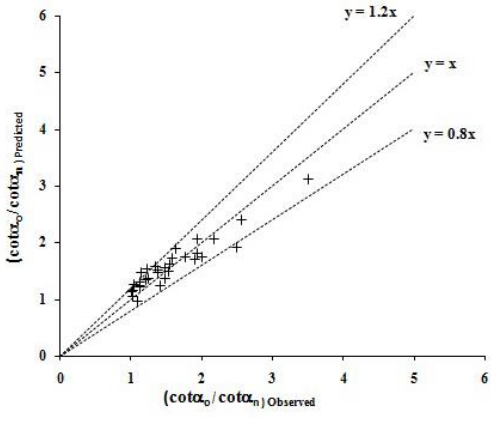

Figure17. Validation of Eq. (19) to determine the equilibrium downstream side slope of the barriers in distractive floods

CONCLUSION

A large number of tests were carried out to investigate slope stability and the failure process of rock-fill barriers. Results determined that water depth upstream of a barrier increased by decreasing the downstream side slope; i.e. with increasing dimensions of the barrier. It was also determined that maximum discharge per unit width of a barrier increases with an increase in the size of stone or a decrease in the downstream side slope, while it decreases with an increase in standard deviation of the stones. Results also determined that those barriers composed of stones with bigger standard deviation had less deformation than those made of stones with lower standard deviation. Equations were provided to determine the depth of flow in upstream sides of barriers, the maximum flow under which barriers remained stable, and for downstream stable side slopes. Comparison of results obtained from these experiments with those obtained from introduced equations in this paper indicated that there was reasonable agreement between the two groups of results, which shows that the new equations introduced in this study have a reasonable level of accuracy for determining the desired parameters.

ACKNOWLEDGMENT

Laboratory tests in this research were carried out in Soil Conservation and Watershed Management Research Institute (SCWMRI), so the authors would like to express their sincere thanks for this collaboration.

REFERENCES

Chanson H. (2009). Embankment Overtopping Protections System and Earth Dam Spillways, in "Dams: Impact, Stability and Design". Hayes, W.P., Barnes, M.C., Nova Science Publishers, Hauppauge NY, USA, 101-132.

Hansen D and Bari R. (2002). Uncertainty in Water Surface Profile of Buried Stream Flowing under Coarse Material. Journal of Hydraulic Engineering 128(8), 761-773.

Herrera N.M., Felton, G.K., (1991). Hydraulic of flow through a rockfill dam using sediment-Free water. Journal of Hydraulic Engineering 34(3), 871-875.

Heydari M., Hosseinzadeh Talaee, P., (2011). Prediction of flow through rockfill dams using a neuro-fuzzy computing technique. Journal of Mathematics and Computer Science 2(3), 515-528.

Lenzi (2002). Stream bed stabilization using boulder check dams that mimic step-pool morphology features in Northern Italy. Journal of Geomorphology 45, 243-260.

Leu, J. M., Chan, H. C., Chu, M. S. (2008). Comparison of turbulent flow over solid and porous structures mounted on the bottom of a rectangular channel. Journal of Flow Measurement and Instrumentation 19(6), 331-337.

Li, B., Garga, V. K., Davies, M. H. (1998). Relationship for Non-darcy Flow in Rockfill. Journal of Hydraulic Engineering 124(2), 206-212.

Samani M. V., Heydari J.M. (2007). Reservoir Routing through Successive Rockfill Detention. Journal of Agriculture Science Technology 9, 317-326.

Maeno, S., Michioku, K., Morinaga. S., Ohnishi T., (2002). Hydraulic characteristics of a rubble mound weir and its failure process. 5th ICHE (Advances in Hydro-Science and Engineering) Conference. Warsaw University of Technology, POLAND, Theme D (CD-ROM).

Michioku, K., Maeno, S., Furusawa, T., Haneda, M., (2005). Discharge through a permeable rubble mound weir. Journal of Hydraulic Engineering 131(1), 1-10.

Mohamed, H. I. (2010). Flow over Gabion Weirs. Journal of Irrigation and Drainage Engineering 136(8), 573-577.

Mousavi, S.A., Amiri-Tokaldany, E., Davoudi, M.H., (2011). A Relationships to Determine the Critical Hydraulic Gradient and No cohesive Sediment Transport Discharge in Rockfill Dams. Research Journal of Environmental Sciences 5, 399-413.

Nazemi. A, Shui. L.T., Davoudi, M.H, Halim, A and Ahmad, D. (2011). Critical Hydraulic Gradient of Non-cohesive Suspended Sediment Laden Flow Through Pervious Rockfill Dam. Australian Journal of Basic and Applied Sciences 5(7), 1119-1126.

Sidiropoulou MG., Moutsopoulos KN, Tsihrintzis VA., (2007). Determination of Forchheimer equation coefficients a and b. Journal of Hydrological Processes 21(4), 534 – 554.

Streeter V.L., Wylie EB (1998). Fluid Mechanics. McGraw-Hill, London.

Yalin M. (1971). Theory of hydraulic models. Macmillan, London.

Zeng Z., Grigg R. B., (2006). A Criterion for Non-Darcy Flow in Porous Media. Journal of Transport in Porous Media 63(1), 57–69.